Graduate School of Pure and Applied Sciences

Optical Coherence Tomography Based Tissue Dynamics Imaging Method and Its Application to Tumor Spheroid Evaluation

（光コヒーレンス・トモグラフィーを用いた組織動態イメージング法とその腫瘍スフェロイド評価への応用）

Ibrahim Gamal Abdelsadek Hossein

Doctoral Program in Applied Physics
Student ID Number 201930100
Doctor of Philosophy in Engineering
Advised by Yoshiaki Yasuno

Abstract

1. Introduction

Cancer is one of the most fatal diseases worldwide[1]. Cancer type varies from patient to patient based one which cell type became cancerous and has an excessive growth rate[2]. Survival rates from cancer can be increased by early detection and optimal selection of anti-cancer drugs for individual patients. Mimicking the in vivo solid tumors by ex vivo culturing of patient-derived cancer cells to form a three-dimensional (3-D) multi-cellular tissue called tumor spheroid[3,4] is useful for anti-cancer drug investigations by measuring the tumor spheroid responses to particular drugs[5–7].

Assessments of tumor spheroids drug response can be performed by several conventional methods such as staining histology[8], fluorescence microscopy[9–11], and time-course tracking of alterations in tissue morphology through microscopic imaging[12]. Although these methods are the gold standards, they have several limitations. Histology is destructive because it requires the tissue to be sliced, which may damage the tissue's micro structures and even alter the functionality of the tumor cells. In addition, it provides 2D images, which are not sufficient for the evaluation of 3D spheroids. Fluorescence microscopic imaging requires the use of exogenous contrast agents (markers), which will then disturb the cellular environment. In addition, deep tissue imaging cannot be performed by fluorescence microscopy because of its limited imaging penetration depth, which make the method not sufficient for the evaluation of thick 3-D tumor spheroids. Morphology imaging based on bright field microscopy has weak tissue specificity and the method is not really quantitative.

The limitations of the conventional methods described above are summarized as follows. First, these methods are invasive. Second, these methods have a limited imaging penetration depth. Third, these methods do not have a volumetric (3-D) imaging capability. These limitations can be partially overcome by using optical coherence tomography (OCT)[13]. OCT is a nondestructive, label-free, and volumetric imaging modality with an imaging depth of a few millimeters. A microscopic version of OCT called optical coherence microscopy (OCM) has been used previously to perform cellular-scale imaging[14–16].

However, conventional OCM can only visualize the morphology of the samples. Therefore, OCM is also not suitable for the spheroid evaluation. To enable use of OCM as a spheroid evaluation tool, it is necessary

to extend the contrasts of OCM. Polarization-sensitive OCT has been shown to give specific contrasts for collagen and melanin[17–20]. Attenuation coefficient (AC) imaging has proved to be sensitive to tissue density[21,22]. In addition, optical coherence electrography can assess the mechanical properties of samples[23–25]. However, these contrast extensions are not sensitive for the tissue viability evaluation.

In this project, we developed a new technology so-called "dynamics OCT", which visualizes and quantifies the subcellular motility, which is closely related to the tissue viability and tissue metabolic activity. The developed method involves the cross-sectional and three-dimensional imaging of the tissue viability. The developed dynamics OCT method was capable for visualization and quantification of the human derived tumor spheroid's tissue viability and its time-course alterations over tens of hours. In addition, the drug response evaluation of the tumor spheroid has been successfully visualized and quantified using the proposed method.

The presented method has several advantages. At first, it is based only on OCT intensity and hence it is compatible with standard speed OCT and doesn't need any hardware extensions of OCT system. Second, is the short measurement time, where 2D cross-sectional dynamics tomography can be captured in 4.48 seconds and 3D OCT volume of 128 different locations in the tissue is captured in 52.4 seconds. Third, is this method visualizes the tissue viability in a totally label-free manner.

The project has been done in two principle phases as presented in Sections 2 and 3.

2. Cross-sectional dynamics imaging

2.1. Method.

The cross-sectional dynamics imaging was performed by combining the rapid sequential acquisition of the OCT B-scans at the same location in the tissue (350 B-scans in 4.48 s used in this study) and two developed signal analysis algorithms[26].

The first algorithm, is logarithmic intensity variance (LIV), which is the time variance of the log-scale OCT intensity as shown in Eq. (1).

$$\text{LIV}(x,z) = \frac{1}{N} \sum_{i=0}^{N-1} [I_{dB}(x,z,t_i) - \langle I_{dB}\rangle_t]^2, (1)$$

where $I_{dB}(x,z,t_i)$ is the logarithmic OCT intensity in a dB scale, x and z are lateral and axial positions, t_i is the acquisition time point of i-th B-scan, N is the total number of B-scans, and $\langle I_{dB}\rangle_t$ is the average over the acquisition time t. LIV accounts for the magnitude of signal fluctuations, but it does not account for the speed of the tissue dynamics.

The second algorithm is the OCT correlation decay speed (OCDS), which quantifies the slope of autocorrelation decay curve of the logarithmic (dB) scale OCT time-sequence. The auto correlation $\rho_A(\tau_i, x, z)$ has been computed as shown in Eq. (2).

$$\rho_A(\tau_i, x, z) = \frac{Cov[I_{dB}(x,z,t_i), I_{dB}(x,z,t_i + \tau_i)]}{Var[I_{dB}(x,z,t_i)] \times Var[I_{dB}(x,z,t_i + \tau_i)]}, \quad (2)$$

where Cov in the numerator represents the covariance between $I_{dB}(x,z,t_i)$ and $I_{dB}(x,z,t_i + \tau_i)$, and $Var[]$ represents the variance. τ_i is the delay time defined as $i\Delta t$, where i is an integer variable and Δt is the B-scan repetition time, it is 12.8 ms in our particular case.

OCDS has two variations based on the time delay range where the slope computation was performed. For example, early ODCS (OSDS$_e$) is computed at the delay range of [12.8, 64 ms] and it is sensitive for the fast dynamics of the tissue. Late OCDS (OCDS$_l$) is computed at late delay times [64, 627.2 ms] and is sensitive for slow dynamics of the tissue.

The OCT measurement have been done using a polarization sensitive swept source OCT system with central wavelength of 1.3 μm and scanning speed of 50 kHz[27]. The system provides and an axial and lateral resolutions of 14 μm and 19 μm, respectively. Although, our system is polarization sensitive, its polarization sensitivity was not used in this study. Only the OCT intensity average of the four polarizations channels of the system is used for dynamics imaging.

The utility of the cross-sectional dynamics imaging method has been investigated for the human breast cancer spheroids (MCF-7 cell line). Two studies have been organized for this purpose. The first study involves the time course evaluation of the MCF-7 spheroid for 24 hours as presented in Section 2.1. The second study involves the cross-sectional drug response evaluation of the MCF-7 spheroid to an anticancer drug so-called paclitaxel (also known as Taxol) as presented in Section 2.2.

2.2. Study 1: cross-sectional time course evaluation of MCF-7 spheroid

Figure 1 summarizes the time course evaluation of MCF-7 spheroid. The column index represents the measurement time point, while the row index represents the measured quantity. By observing the OCT time course [Fig.1 (a)], we cannot see a clear difference over the time.

On the other hand, the LIV images [Fig.1 (b)] showed that, at the early time points, LIV is large (green) at the spheroid periphery, while it is low (red) at the center. At the later time points, the high LIV at the periphery faded. It is known that the necrosis of large spheroids starts at their center because of the lack of the oxygen and other nutrient supply[4,28]. This finding in the LIV is consistent with this necrotic process of the spheroids.

The OSDS$_e$ images [Fig.1 (c)] show that at the early time points, the center region of the spheroid shows fast dynamics (green). At the later time points, the entire region of the spheroid exhibits fast dynamics (green). It was previously reported that the necrotic process in the spheroid exhibited fast decorrelation of the OCT signal[29]. This is consistent with the present finding here.

Fig.1: Longitudinal dynamics visualization of an MCF7 spheroid. The first to fourth rows show time-course images of (a) OCT intensity, (b) LIV, (c) OSDS$_e$, and (d) OCDS$_l$.

The OCDS$_l$ images [Fig.1 (d)] show an opposite contrast to that of the OSDS$_e$. Specifically, at the 0 h time point, the peripheral region shows significant correlation decay (green), while it becomes dim at the later time points. At all the time points, the center region appears in red. This would be because the correlation already
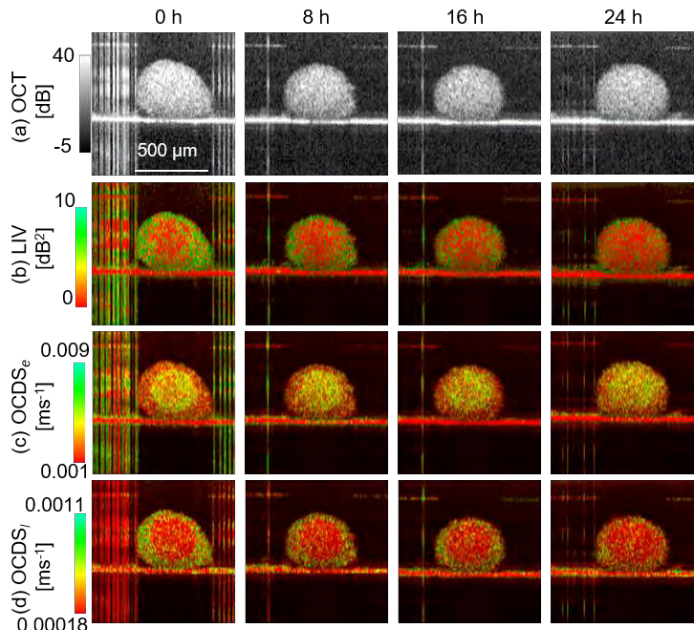
decayed at an early delay time as it was indicated by the green color in the OSDS$_e$ images [Fig.1 (c)].

These results suggest that proposed cross-sectional dynamics imaging successfully visualized the time course alteration in the MCF-7 spheroid tissue viability and its necrotic activity.

2.3. Study 2: cross-sectional drug response evaluation of MCF-7 spheroid

The drug response evaluation of MCF-7 spheroids treated with 5, 50, and 500 nM in addition to control case (0 nM) is shown in Fig. 2. In the control case, the peripheral region of the spheroid exhibits a high LIV, low OSDS$_e$, and high OCDS$_l$. These appearances indicate that the cells at the periphery are still alive, while those within the central region are in the necrotic process. The fluorescence image is consistent with these findings of dynamics images because the peripheral cells exhibit green fluorescence (living cells) and the center cells exhibit red fluorescence (dead cells).

The spheroid with 5-nM Paclitaxel (second column) show similar appearance with the control except that the red appearance in the fluorescence image forms large clusters, LIV image shows a moderate clustering appearance of low dynamics (red) within the spheroid, OSDS$_e$ image shows clear clusters of fast correlation decay (colored yellow to green).

Fig.2: Drug response of MCF7 spheroids. The first to fifth rows represent the results from (a) fluorescence microscopy, (b) the OCT intensity image, (c) the LIV, (d) the OCDS$_e$, and (e) the OCDS$_l$. The fluorescence microscopy images are en face images, while the other images are all cross-sectional images. The columns represent the paclitaxel concentrations.

The dynamics images of the 50- and 500-nM cases show opposite contrasts to the control and 5-nM cases. Specifically, the external parts of the spheroid show low LIV (red), high OSDS$_e$ (green), and low OCDS$_l$ (red) as depicted by the white arrows and circle, while the internal parts exhibit high LIV (green), low OSDS$_e$ (red), and high OCDS$_l$ (green). Because we believe that the combination of low LIV and high OSDS$_e$ are indicators of the necrotic process, these appearances can be interpreted as the necrotic process occurring at the outer part of the spheroid. And it might be due to the high concentrations of Taxol. Consistent appearances can be found in the fluorescence images, where the outer and inner parts of the spheroid exhibit red and green fluorescence, respectively.

The results presented in Fig. 2 show that the proposed cross-sectional dynamics imaging method might be useful for tumor spheroid drug response investigation and it can complement fluorescence imaging and become a useful tool for precision medicine and tumor spheroid-based drug screening.
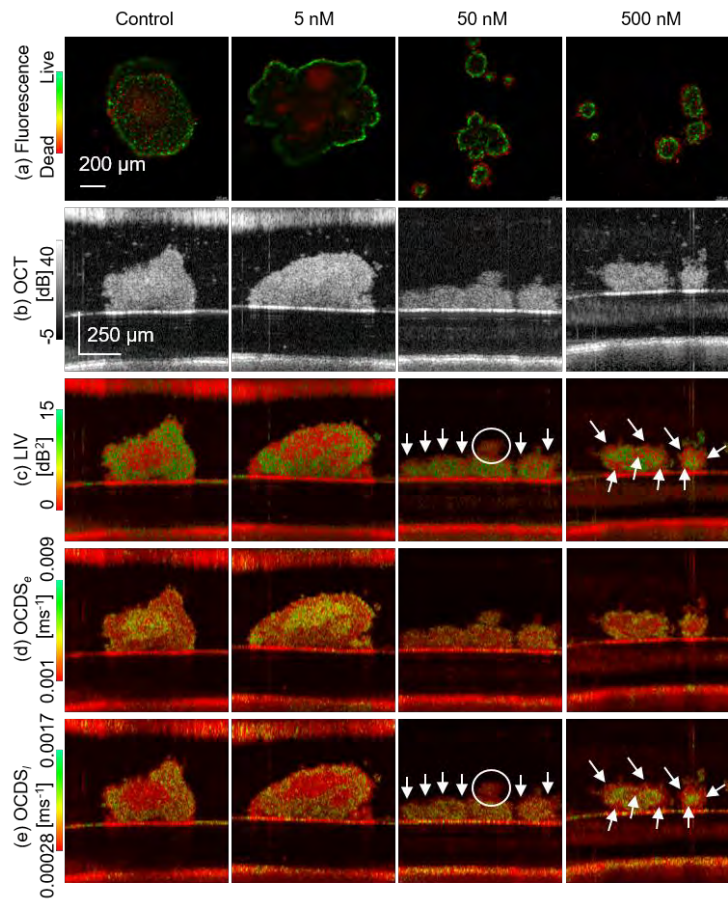
3. Three-dimensional dynamics imaging

3.1. Method

In this study we presented the development of our method discussed in Section 1 to be capable for of 3-D dynamics imaging[30]. At the end of the cross-sectional dynamics imaging study (Section 1), we did an optimization analysis of the number of frames and the acquisition time window, which is required for tissue dynamics imaging. It was found that 17 or 33 frames at each location in the tissue were sufficient for dynamics imaging as far as the time window is large as 6.55s[26]. From this perspective, we designed a new custom made 3-D OCT scanning protocol, which allows the acquisition of OCT volume consists of 128 locations in the tissue in less than a minute (exactly 52.5 s). This protocol repeats 32 B-scans at each location in the tissue in 6.55 s, where the B-scan repetition time was 204.8 ms[30].

The OCT signal analysis framework was similar to that was used in phase 1 study. Where the 3-D magnitude of the tissue dynamics has been visualized by computing the LIV at each location using the acquired 32 B-scans. The slow dynamics of the tissue has been visualized using $OCDS_l$, but in this case as the time separation between frames became larger and the number of points to compute the correlation became smaller (32 B-scans), we computed the autocorrelation using spatially extended kernel with dimensions of (2×4 pixels) in axial and lateral directions, respectively. Then the autocorrelation decay slope ($OCDS_l$) is computed at a delay range of [204.8, 1228.8 ms].

The utility our developed 3-D dynamics OCT has been investigated using two studies as presented in Sections 3.1 and 3.2, respectively.

3.2. Study1: 3D time-course evaluation of MCF-7 spheroid

This study involves the time course evaluation of MCF-7 spheroid tissue viability. Where the spheroid has been cultured by seeding 1,000 human breast tumor cells for two weeks then extracted from the tissue culture environment and measured using 3-D OCT longitudinally.

Figures 3 and 4 represents the time course LIV and $OCDS_l$ visualization of the MCF7 spheroid measured at three time points (0 h, 16 h, and 20 h). At 0-hr time point the volume rendering [Fig. 3 (a) and Fig.4 (a)] shows a clear low LIV and $OCDS_l$ signals (red) at the spheroid core and this appearance is related to the well-known tumor spheroid necrotic core, while the spheroid periphery shows high LIV and $OCDS_l$ signals (green), which highlights the living cancer cells at the spheroid periphery[4,28]. The same appearances are appeared in cross-sectional views [Figs. 3 (b-d) and 4 (b-d)]. The high LIV and $OCDS_l$ are faded along the time and almost all the spheroid volumes show tissue necrotic appearance (low LIV and $OCDS_l$). This tissue necrosis is a kind of cell death and it could be occurred because of the lack of nutrient supply for the cancer cells as the measurement was done in room temperature and without tissue culture condition.

3.3. Study 2: 3D drug-response evaluation of MCF-7 spheroid)

This study involves the drug response evaluation of the MCF-7 spheroid. Human breast cancer cells have been seeded in three wells of 96 well-plate (500 cells/ well) to form three spheroids after four days. On the fourth day the three spheroids have been treated with three concentrations (0 µM, 0.1 µM, and 1 µM) of anti-cancer drug called Taxol. The treatment was done for three days, then the fluorescence microscopy and the 3-
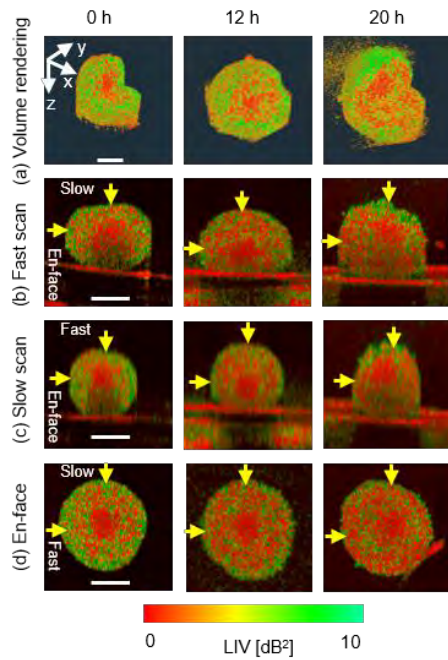
D OCT measurement were performed.

Fig.3: Time-course LIV of MCF-7 spheroid. (a) the cut-away volume rendering. (b-d) represents the cross-section along different directions in the tissue. The scale bars represent 200 μm.
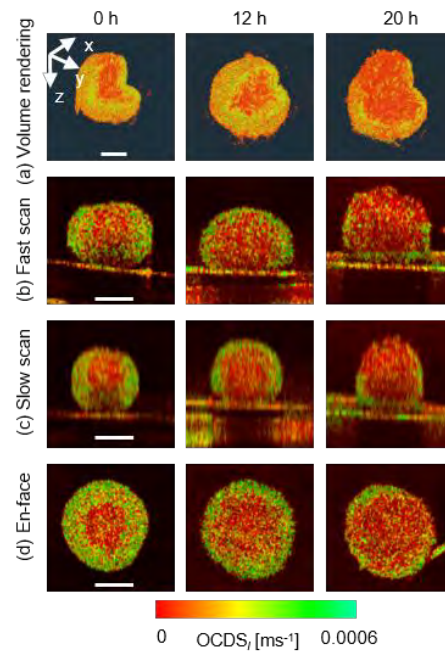
Fig.4: Time-course OCDS$_l$ of MCF-7 spheroid. The images are displayed in the same manner as Fig. 3.

Figure 5 represents the drug response visualization of the MCF-spheroid. The first and second rows [Fig.5 (a) and (b)] represents the LIV cross-sectional and enface images, the third and fourth rows [Fig.5 (c) and (d)] LIV cross-sectional and enface OCDS$_l$ images, while the fifth to sixth rows [Fig.5 (e) and (f)] represents the composite fluorescence image of living cells (green) and dead cells (red) and the dead cells only (red) fluorescence image. The column index represents the drug concentrations.

At the control (0 μM) case the LIV and OCDS$_l$ images shows a diffusive appearance of low (red) and high (green) signal which the majority of high signal (green) appearance. The fluorescence image shows dead cells at the spheroid center surrounded by living cells at the spheroid periphery, which corresponds to the low and high LIV signals.

By increasing the drug concentrations, the high LIV and OCDS$_l$ signals are fading along the drug concentration until covering almost all the spheroid region with low LIV and OCDS$_l$ (red) at 1 μM case. On the other hand, fluorescence images show an increase of the dead cells in almost all the spheroid region.

The increase of the low LIV, low OCDS$_l$, and dead cells fluorescence signals might indicate the cancer cell death under the application of the drug.

The presented results in Section 3; study 1 and study 2 shows that the proposed 3-D dynamics OCT successfully visualized the time-course alteration of the tumor spheroid tissue viability. In addition, the drug response of the MCF-7 spheroid has been successfully visualized in a totally label-free manner.

4. **Summary and conclusion**

In summary we proposed a label-free optical coherence tomography-based cross-sectional and three-dimensional tissue dynamics imaging method for the human derived tumor spheroid evaluation. The utility of

the proposed methods has been investigated for the time-course evaluation of the human breast cancer spheroid (MCF-7 cell line). In addition, the drug response of the MCF-7 spheroid has been visualized.

From the presented results we conclude that our method is useful for the evaluation of tumor spheroid time-course tissue viability alterations. In addition, it is useful for the evaluation of tumor spheroid anti-cancer drug response. Our method is totally label free and non-destructive. So, it might become a useful tool for precision medicine research and it might complement other conventional methods for tumor spheroid based drug investigations.

Fig.5: Drug response visualization of the MCF-7 spheroid. (a and b) represents the cross-section and enface LIV images. (c and d) represents the cross-section and enface OCDS$_l$ images. (d and e) represents the composite and the single channel fluorescence images, respectively. The scale bars represent 200 μm.

References

1. R. L. Siegel, K. D. Miller, and A. Jemal, "Cancer statistics, 2020," CA. Cancer J. Clin. **70**(1), 7–30 (2020).

2. G. M. Cooper, *The Cell: A Molecular Approach* (ASM Press ; Sinauer Associates, 2000).

3. J. M. Yuhas, A. P. Li, A. O. Martinez, and A. J. Ladman, "A Simplified Method for Production and Growth of Multicellular Tumor Spheroids," Cancer Res. **37**(10), 3639–3643 (1977).

4. F. Hirschhaeuser, H. Menne, C. Dittfeld, J. West, W. Mueller-Klieser, and L. A. Kunz-Schughart, "Multicellular tumor spheroids: An underestimated tool is catching up again," J. Biotechnol. **148**(1), 3–15 (2010).

5. X. Gong, C. Lin, J. Cheng, J. Su, H. Zhao, T. Liu, X. Wen, and P. Zhao, "Generation of Multicellular Tumor Spheroids with Microwell-Based Agarose Scaffolds for Drug Testing," PLOS ONE **10**(6), e0130348 (2015).

6. B. Galateanu, A. Hudita, C. Negrei, R.-M. Ion, M. Costache, M. Stan, D. Nikitovic, A. W. Hayes, D. A. Spandidos, A. M. Tsatsakis, and O. Ginghina, "Impact of multicellular tumor spheroids as an in vivo-like tumor model on anticancer drug response," Int. J. Oncol. **48**(6), 2295–2302 (2016).

7. S. Sant and P. A. Johnston, "The production of 3D tumor spheroids for cancer drug discovery," Drug Discov. Today Technol. **23**, 27–36 (2017).
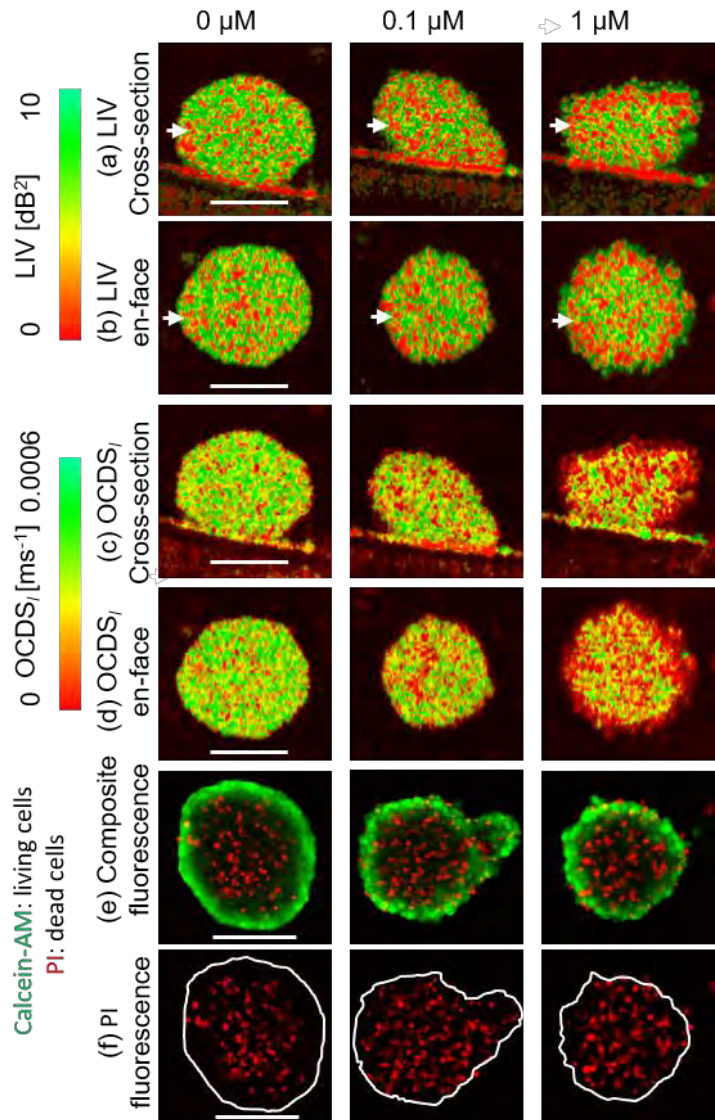
8. S. Plummer, S. Wallace, G. Ball, R. Lloyd, P. Schiapparelli, A. Quiñones-Hinojosa, T. Hartung, and D. Pamies, "A Human iPSC-derived 3D platform using primary brain cancer cells to study drug development and personalized medicine," Sci. Rep. **9**(1), 1407 (2019).

9. F. Mittler, P. Obeïd, A. V. Rulina, V. Haguet, X. Gidrol, and M. Y. Balakirev, "High-Content Monitoring of Drug Effects in a 3D Spheroid Model," Front. Oncol. **7**, (2017).

10. M. M. Lukina, V. V. Dudenkova, N. I. Ignatova, I. N. Druzhkova, L. E. Shimolina, E. V. Zagaynova, and M. V. Shirmanova, "Metabolic cofactors NAD(P)H and FAD as potential indicators of cancer cell response to chemotherapy with paclitaxel," Biochim. Biophys. Acta BBA - Gen. Subj. **1862**(8), 1693–1700 (2018).

11. W. Yang, S. Cai, Z. Yuan, Y. Lai, H. Yu, Y. Wang, and L. Liu, "Mask-free generation of multicellular 3D heterospheroids array for high-throughput combinatorial anti-cancer drug screening," Mater. Des. **183**, 108182 (2019).

12. D. A. Seleci, M. Seleci, F. Stahl, and T. Scheper, "Tumor homing and penetrating peptide-conjugated niosomes as multi-drug carriers for tumor-targeted drug delivery," RSC Adv. **7**(53), 33378–33384 (2017).

13. W. Drexler and J. G. Fujimoto, eds., *Optical Coherence Tomography: Technology and Applications*, 2nd ed. (Springer International Publishing, 2015).

14. W. Drexler, U. Morgner, F. X. Kärtner, C. Pitris, S. A. Boppart, X. D. Li, E. P. Ippen, and J. G. Fujimoto, "In vivo ultrahigh-resolution optical coherence tomography," Opt. Lett. **24**(17), 1221–1223 (1999).

15. A. Dubois, G. Moneron, K. Grieve, and A. C. Boccara, "Three-dimensional cellular-level imaging using full-field optical coherence tomography," Phys. Med. Biol. **49**(7), 1227–1234 (2004).

16. A. D. Aguirre, C. Zhou, H.-C. Lee, O. O. Ahsen, and J. G. Fujimoto, "Optical Coherence Microscopy," in *Optical Coherence Tomography: Technology and Applications*, W. Drexler and J. G. Fujimoto, eds. (Springer International Publishing, 2015), pp. 865–911.

17. E. Götzinger, M. Pircher, W. Geitzenauer, C. Ahlers, B. Baumann, S. Michels, U. Schmidt-Erfurth, and C. K. Hitzenberger, "Retinal pigment epithelium segmentation by polarization sensitive optical coherence tomography," Opt. Express **16**(21), 16410–16422 (2008).

18. S. Makita, Y.-J. Hong, M. Miura, and Y. Yasuno, "Degree of polarization uniformity with high noise immunity using polarization-sensitive optical coherence tomography," Opt. Lett. **39**(24), 6783–6786 (2014).

19. S. Sugiyama, Y.-J. Hong, D. Kasaragod, S. Makita, S. Uematsu, Y. Ikuno, M. Miura, and Y. Yasuno, "Birefringence imaging of posterior eye by multi-functional Jones matrix optical coherence tomography," Biomed. Opt. Express **6**(12), 4951–4974 (2015).

20. J. F. de Boer, C. K. Hitzenberger, and Y. Yasuno, "Polarization sensitive optical coherence tomography – a review [Invited]," Biomed. Opt. Express **8**(3), 1838–1873 (2017).

21. D. J. Faber, F. J. van der Meer, M. C. G. Aalders, and T. G. van Leeuwen, "Quantitative measurement of attenuation coefficients of weakly scattering media using optical coherence tomography," Opt. Express **12**(19), 4353–4365 (2004).

22. K. A. Vermeer, J. Mo, J. J. A. Weda, H. G. Lemij, and J. F. de Boer, "Depth-resolved model-based reconstruction of attenuation coefficients in optical coherence tomography," Biomed. Opt. Express **5**(1), 322–337 (2014).

23. B. F. Kennedy, R. A. McLaughlin, K. M. Kennedy, L. Chin, A. Curatolo, A. Tien, B. Latham, C. M.

Saunders, and D. D. Sampson, "Optical coherence micro-elastography: mechanical-contrast imaging of tissue microstructure," Biomed. Opt. Express **5**(7), 2113–2124 (2014).

24. K. V. Larin and D. D. Sampson, "Optical coherence elastography – OCT at work in tissue biomechanics [Invited]," Biomed. Opt. Express **8**(2), 1172–1202 (2017).

25. Y. Li, S. Moon, J. J. Chen, Z. Zhu, and Z. Chen, "Ultrahigh-sensitive optical coherence elastography," Light Sci. Appl. **9**(1), 58 (2020).

26. I. A. El-Sadek, A. Miyazawa, L. T.-W. Shen, S. Makita, S. Fukuda, S. Fukuda, T. Yamashita, Y. Oka, P. Mukherjee, S. Matsusaka, T. Oshika, H. Kano, and Y. Yasuno, "Optical coherence tomography-based tissue dynamics imaging for longitudinal and drug response evaluation of tumor spheroids," Biomed. Opt. Express **11**(11), 6231–6248 (2020).

27. E. Li, S. Makita, Y.-J. Hong, D. Kasaragod, and Y. Yasuno, "Three-dimensional multi-contrast imaging of in vivo human skin by Jones matrix optical coherence tomography," Biomed. Opt. Express **8**(3), 1290–1305 (2017).

28. E. C. Costa, A. F. Moreira, D. de Melo-Diogo, V. M. Gaspar, M. P. Carvalho, and I. J. Correia, "3D tumor spheroids: an overview on the tools and techniques used for their analysis," Biotechnol. Adv. **34**(8), 1427–1441 (2016).

29. G. Farhat, A. Mariampillai, V. X. D. Yang, G. J. Czarnota, and M. C. Kolios, "Optical coherence tomography speckle decorrelation for detecting cell death," in *Biomedical Applications of Light Scattering V* (International Society for Optics and Photonics, 2011), **7907**, p. 790710.

30. I. A. El-Sadek, A. Miyazawa, L. T.-W. Shen, S. Makita, P. Mukherjee, A. Lichtenegger, S. Matsusaka, and Y. Yasuno, "Three-dimensional dynamics optical coherence tomography for tumor spheroid evaluation," Biomed. Opt. Express **12**(11), 6844–6863 (2021).